ELSEVIER

International Journal of Mass Spectrometry 194 (2000) 133–143

International Journal of Mass Spectrometry

Measurement of the proton affinities of some methyl substituted pyrimidines via the kinetic method on a pentaquadrupole mass spectrometer

Peter D. Thomas[a], Richard J.S. Morrison[b,*]

[a]*Aston Laboratory for Mass Spectrometry, Department of Chemistry, Purdue University, West Lafayette, IN 47907-1393, USA*
[b]*Department of Chemistry, Monash University, Clayton, Victoria 3168, Australia*

Received 22 March 1999; accepted 22 June 1999

Abstract

The proton affinities of 4,6-dimethyl-pyrimidine and 4-methyl-pyrimidine have been measured using the kinetic method on a pentaquadrupole mass spectrometer. The experimental affinities are compared with those calculated by ab initio molecular orbital methods. Some unexpected results obtained during this work have been attributed to the formation of the 6-methyl-pyrimidin-4-yl radical and its proton affinity has also been estimated by both theory and experiment. (Int J Mass Spectrom 194 (2000) 133–143) © 2000 Elsevier Science B.V.

Keywords: Tandem mass spectrometry; Pentaquadrupole; Proton affinity; Kinetic method; Pyrimidine

1. Introduction

Tandem mass spectrometry has become a well-established technique in analytical mass spectrometry and gas-phase ion chemistry [1]. Ion trapping instruments, such as the Fourier transform ion cyclotron resonance (FTICR) spectrometer [2] and the quadrupole (or Paul) ion trap [3], offer the advantage of performing several sequential stages of mass spectrometry. Tandem instruments with electrospray or atmospheric pressure chemical ionization sources make use of collisions in the high pressure sampling orifice to perform an extra stage of decomposition [4,5]. Multisector instruments are also capable of several MS stages, though at a cost in terms of analyzer performance [6].

To make use of the full range of possible MS^3 experiments [7] an instrument with three independent analyzers and two collision regions is required. Such an instrument is the pentaquadrupole, an extension of the popular triple quadrupole used in MS^2. The general concepts and applications of pentaquadrupole mass spectrometry are the subject of a comprehensive review article [8].

We have constructed a pentaquadrupole mass spectrometer, that is to our knowledge the fifth such instrument of this type. In this article the instrument is described and its performance via kinetic method [9–11] experiments yielding proton affinities for 4,6-dimethyl-pyrimidine, 4-methyl-pyrimidine, and the 6-methyl-pyrimidin-4-yl radical is demonstrated.

* Corresponding author.

Dedicated to Professor Jim Morrison on the occasion of his 75th birthday.

PII S1387-3806(99)00138-4

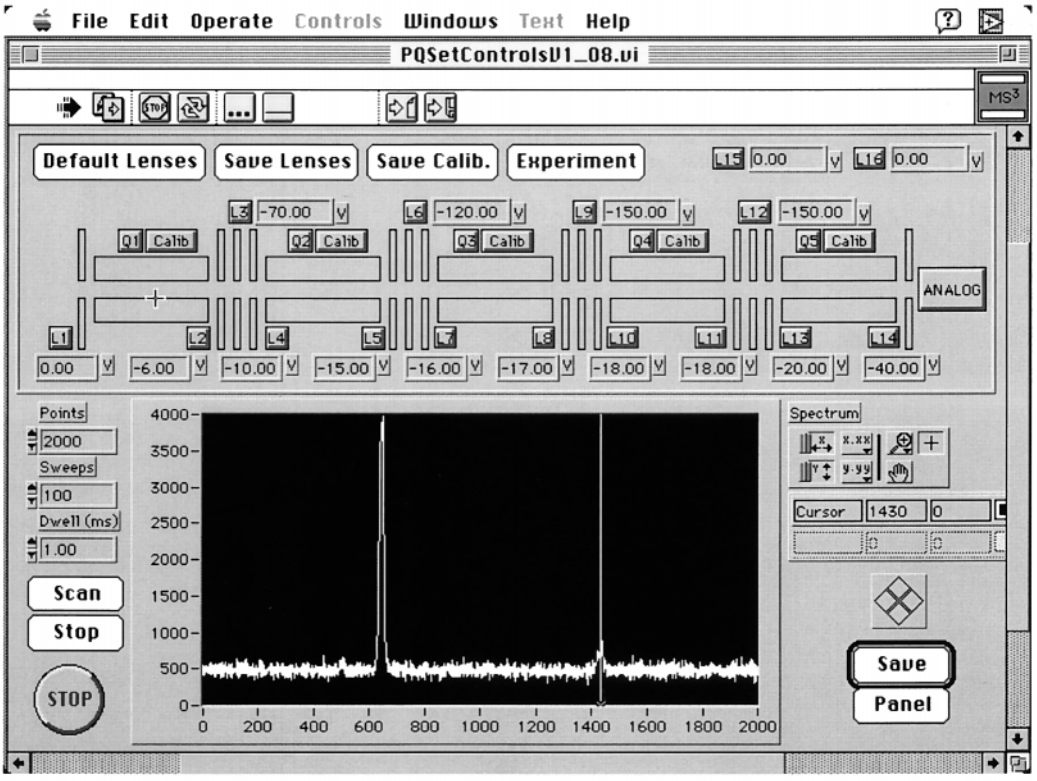

Fig. 1. LabVIEW control panel for the pentaquadrupole mass spectrometer.

2. Instrumentation

The pentaquadrupole used in this work was almost completely homebuilt, and was based on an ion optical rail having five coaxial rod assemblies, each separated by an einzel lens and originally machined at LaTrobe University for Professor Jim Morrison. On the occasion of his retirement Jim kindly donated the rail to our laboratory and we set about incorporating it into a complete instrument.

The control system for this instrument incorporates a number of novel features and is described briefly below; full details can be found elsewhere [12]. Fig. 1 shows the LabVIEW (National Instruments) front panel developed for the instrument. Whereas user interaction takes place from this panel, the actual control functions are implemented from a diagram that in essence is a graphical program created using icons and connecting wires. This diagram issues serially transmitted command strings to a separate control unit that uses a digital signal processor to manage basic functions such as setting lens voltages and scanning the rf generators that drive the quadrupole rods.

In the top third of the panel is a pictorial representation of the instrument. It is arranged from left to right, starting with the ion source and finishing with the detector. In the center of the display is a chart showing the latest spectrum gathered by the instrument. Down the left-hand side are a number of sweep settings. To the right are controls for manipulating the display and saving the data. A large stop button in the bottom left-hand corner terminates the program and shuts down the instrument.

The buttons along the top of the control panel allow setting and saving of standard lens potentials for twelve interquadrupole, one prequad, and one post-quad ion lenses. In addition, a set of quadrupole

calibration parameters is automatically loaded on program initialization; these parameters define the mass, resolution, and ion energy settings for each mass filter as second order functions of the pass mass. Calibration buttons associated with each quadrupole allow user changes to the nine such coefficients for each filter; the full set can also be saved.

An experiment button provides a means to save and restore additional sets of quadrupole operating parameters for common experiments. These parameters include the start/park mass, the scan range, and other key operating modes—operate/standby, positive ion/negative ion, rf-only/rf-dc, and park/scan.

The rf/dc power supplies for the quadrupole rods were built at Monash University, Victoria, Australia. A crystal-controlled Colpitts oscillator provided frequency regulation. This fed a 24 V rf amplifier and a tuned transformer circuit to produce matched sinusoidal waveforms, with a phase separation of 180° and amplitude of 15 V_{p-p}. These drove a MOSFET push–pull amplifier that boosted the current to as high as 1 A. A final tuned circuit developed about 700 V_{rms}, depending on the particular frequency. This output drove the rods and a capacitive voltage divider produced the feedback signal. The feedback signal was compared with the mass control input and used to maintain the correct voltage.

The frequencies for the Q1 and Q3 supplies were set to 1.4 MHz and 1.6 MHz giving effective upper mass limits of 400 u and 250 u, respectively. The Q2 and Q4 frequencies were kept at 1.0 MHz to provide a wide stability band for parent and product ions. Q5 was also operated at 1.0 MHz; this mass filter had an upper mass limit of approximately 1000 u. Typical mass spectra recorded in this work consisted of 2000 points, with a single sweep taking 0.6 s. At 10 points per amu this yields an effective scan rate of 333 *m/z* s^{-1}. Transfer of the data from the digital signal processor to the host computer takes slightly over 1 s at 57.6 kBaud.

The quadrupole rod assemblies in this instrument were supported at each end by Delrin blocks (Dupont, Wilmington, DE), machined so as to fix the rods in the correct geometry. The rods were centerless ground stainless steel, 125 mm long and 8 mm in diameter. The four interquadrupole lens assemblies were three-element aperture types, comprising entrance and exit plates with tubular extensions into the rf fields and a thick focus plate. Lenses were also mounted at the entrance to Q1 and at the exit of Q5.

The aluminum rail supporting the rod assemblies and ion lenses was housed in a cylindrical steel vacuum chamber, 20 cm in diameter and 91.4 cm long. The chamber was pumped by two oil vapor diffusion pumps (Edwards Diffstak 160/700 and Varian VHS-4, using Santovac5 pump oil), each backed by a separate two-stage, oil-sealed, rotary pump (Edwards E2M40 and E2M28, respectively). A third diffusion pump (Edwards Diffstak 63/150) and rotary pump (Javac JDL220) combination evacuated a small tee mounted at the exit of Q5 that housed a model AF521H (ETP) discrete dynode electron multiplier with a rated gain of 10^8 at −2000 V.

Shrouds made from copper sheet isolated the Q2 and Q4 collision cells from the rest of the chamber. A short length of 1/8″ copper tube was soldered into the top of each shroud to admit reagent gas. Connections between these stubs and the reagent gas inlets were made by short lengths of Tygon tubing.

The ion source was taken from a HAL201 residual gas analyzer (Hiden Analytical). It comprised two filaments within a totally enclosed ion volume, plus source and extractor plates. The gas entrance aperture was 6 mm and the source exit aperture was 4 mm. The exit aperture was modified by adding an extra plate with an aperture diameter of 2.8 mm in mechanical and electrical contact with the source plate.

System pressures were measured by two Penning gauges, one mounted near Q4 in the main volume of the chamber (Leybold-Heraeus PenningVac PM 410) and the other mounted within the detector housing (Edwards CP25-K). The base pressure of the main vacuum chamber was about 1×10^{-6} mbar, though after extended periods of pumping, pressures of 7×10^{-7} mbar were achieved. The detector region achieved a base pressure of 1.7×10^{-6} mbar. In some of the experiments described here the chamber pressure increased to 4×10^{-4} mbar because of the gas load from the source and reagent inlets, however

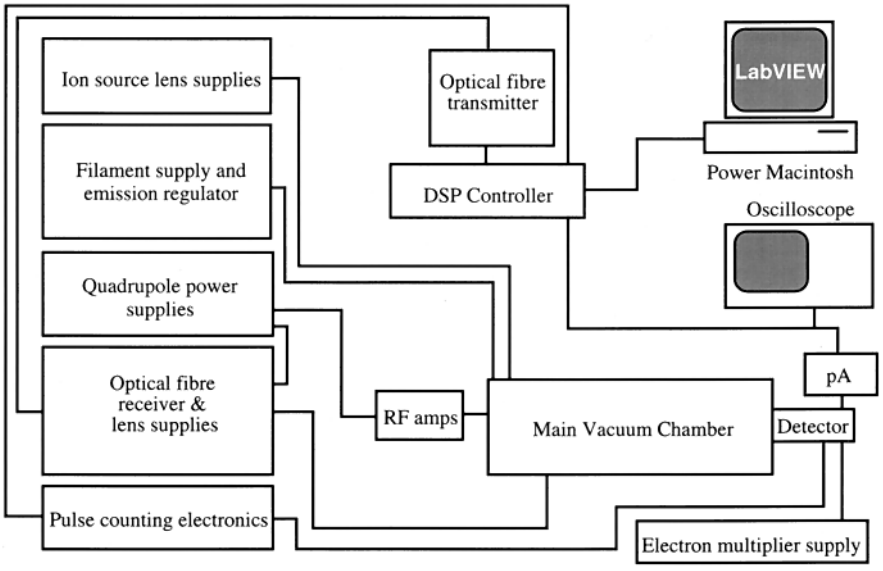

Fig. 2. Block diagram of the pentaquadrupole instrument.

the pressure in the detector region only rose as high as 2×10^{-5} mbar.

Analog signals were measured by a SR570 battery powered picoammeter (Stanford Research Systems) and fed to a HP54603B 60 MHz digital oscilloscope (Hewlett-Packard) for real-time display. Digitized spectra could be saved to a disk directly from the LabVIEW front panel. A block diagram of the full system is shown in Fig. 2.

With all the quadrupoles operating in the rf-only mode, the instrument transmits approximately one tenth of the ion current generated by the ion source. In full MS^3 mode, the transmission drops a further four orders of magnitude. The transmission of the mass filters in mass-selective mode, compared to rf-only mode, is quite low—between 5% and 10%. Given the operating frequencies and physical dimensions of the rods used, this level of performance is to be expected and could easily be improved upon. An extensive investigation of the ion transport in the various regions of this instrument has been carried out using SIMION 3D [13] and these results will be presented in a forthcoming publication.

Source pressures as high as 10^{-2} mbar can be achieved, allowing the formation of $[M + H]^+$ ions by self-chemical ionization (self-CI). The maximum reagent pressure is about 10^{-3} mbar, however the collection efficiency of the reaction regions falls very rapidly at pressures greater than 5×10^{-4} mbar. With the current rf-dc supplies the laboratory collision energy in Q2 and Q4 is restricted to a maximum value of 10 eV and thus collision-induced dissociation (CID) can only deposit a small amount of energy into a selected ion in these regions.

3. Experimental

Proton-bound dimers for the kinetic method experiments were generated by ion/molecule reactions in the second quadrupole of the pentaquadrupole instrument. $[M + H]^+$ ions were produced by self-CI in the ion source and reacted with neutral molecules after selection in Q1. The pole offset for Q2 was set to be about equal to the source potential (+2–3 V). The third quadrupole was used to select the dimer, which was then fragmented by collisions with air from the atmosphere in Q4, and the fragment abundances recorded by scanning Q5. The Q4 pole offset was varied between 0 V and −5 V, resulting in nominal

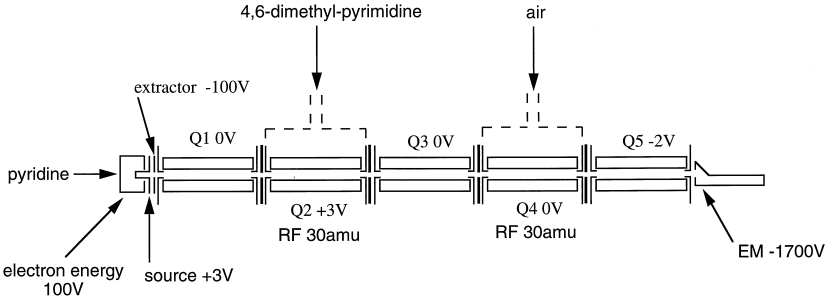

Fig. 3. Typical instrument parameters used in the kinetic method experiments. In the reaction sequence illustrated, protonated pyridine ions are mass selected by Q1, and reacted with 4,6-dimethyl-pyrimidine in Q2. Q3 is tuned to isolate the proton-bound dimer, which undergoes CID with air in Q4. The mass spectrum of fragment ions is recorded by scanning Q5.

collision energies of 3–8 eV in the laboratory reference frame. For the collision of a *m/z* 187 ion on a 28 Da neutral target this equates to energies of 0.4–1.0 eV in the center-of-mass frame. Fig. 3 shows some typical instrument parameters.

Samples were obtained as liquids from Aldrich (Milwaukee, WI) and BDH (Poole, UK) and were used without purification. The liquids were degassed by several freeze–thaw cycles after being transferred to glass bulbs. The source sample was metered from a vacuum line pressure equivalent to the vapor pressure, up to about 10 mbar, through a micrometer gauge needle valve. Sample was added until the chamber pressure, as indicated by the main pressure gauge opposite Q4, reached a value of $2 \sim 6 \times 10^{-5}$ mbar. The Q2 reagent was vaporized in a glass vacuum line and admitted to the chamber via a Granville-Phillips model 203 variable leak valve to a total chamber pressure of around 1×10^{-4} mbar.

Air at atmospheric pressure was admitted to the vacuum line for Q4 and metered through a micrometer gauge needle valve until the main fragment peak was of a similar intensity to the parent, at which point the total pressure was usually about 2×10^{-4} mbar. Several spectra were then recorded for periods ranging up to about 1 h with minimal further adjustment, depending on the amount of sample available. Most spectra used to measure fragment ratios were averages of 100 or 200 sweeps. A spectrum comprising 100 coadded scans of 2000 points each at a picoammeter setting of 1 nA/V and a dwell time of 1 ms required approximately 4 min.

The fragment ratios were calculated by integrating the areas under the respective peaks. Initially this was facilitated by the spreadsheet program Kaleidagraph (Synergy Software, Reading, PA) but later with the aid of a custom written LabVIEW peak detection and integration program. Ratios obtained by the two methods for the same spectrum differed by less than 1%. In general, peaks were integrated over a 2 or 4 *m/z* window centered on the peak maximum, depending on the resolution of the spectrum.

Ab initio proton affinities (at 298 K) were calculated for the unknowns and for a number of other compounds using GAUSSIAN 94 [14]. These calculations were performed on a 12 CPU SGI (Silicon Graphics International) Power Challenge R10000 high performance computer.

4. Results and discussion

4.1. Kinetic method experiments

The kinetic method is a means of obtaining relative proton affinities from fragment ion abundance ratios in dissociations of proton-bound dimers $A \ldots H^+ \ldots B$. Other thermochemical data can be obtained in analogous experiments involving different binding species [10,11]. Proton affinities for 4,6-dimethyl-pyrimidine and 4-methyl-pyrimidine were obtained from kinetic method experiments using the pentaquadrupole mass spectrometer described above. The following compounds: pyridine, 4-methyl-pyri-

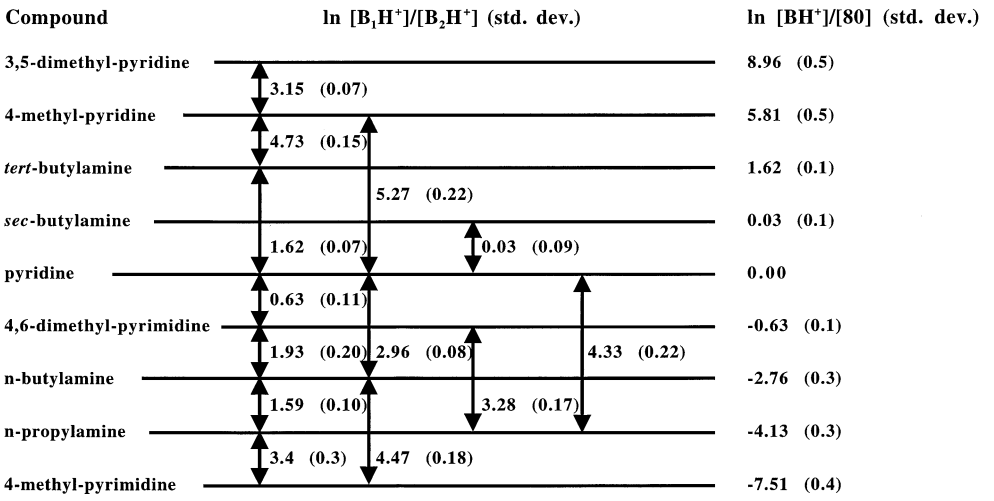

Fig. 4. Logarithms of fragment ratios for all reaction partners at E_{lab} = 3 eV.

dine (4-picoline), 3,5-dimethyl-pyridine (3,5-lutidine), *n*-propylamine, *n*-butylamine, *sec*-butylamine, and *tert*-butylamine, were used as reference species. The use of these compounds as standards is not ideal because they represent at least two distinct classes of amines and the kinetic method is best applied when all species belong to a single class. However, the selected set was desirable from an instrument performance standpoint and the tabulated protonation entropies are all reasonably close to zero [15]. Not all the references were paired with the unknowns; instead, where necessary the results of two or more individual experiments were combined in a stair-step fashion to provide an expected relative abundance ratio. Proton affinities for the references were taken from the recent compilation of Hunter and Lias [15].

The natural logarithms of the fragment ratios obtained at a collision energy of 3 eV in the laboratory frame for all of the pairings studied are shown in Fig. 4. Data for each pair represent the average of at least three separate experiments with the standard deviation shown in parentheses. These were combined to produce the unified scale on the right by averaging the results obtained by the various possible combinations of steps. A similar set of data was obtained at a collision energy of 8 eV.

The data at both 3 eV and 8 eV collision energy are displayed in Figs. 5 and 6, with the scale zero adjusted to 4,6-dimethyl-pyrimidine and 4-methyl-pyrimidine, respectively. The points have been fitted to Eq. (1):

$$\ln(\text{ratio}) = \frac{\text{PA(ref)} - \text{PA(unknown)}}{RT_{\text{eff}}} \quad (1)$$

with R, the gas constant, in kJ mol^{-1} K^{-1} and with the gradient allowing a value to be determined for T_{eff}, the effective temperature in K. The proton affinities derived from this procedure are as follows:

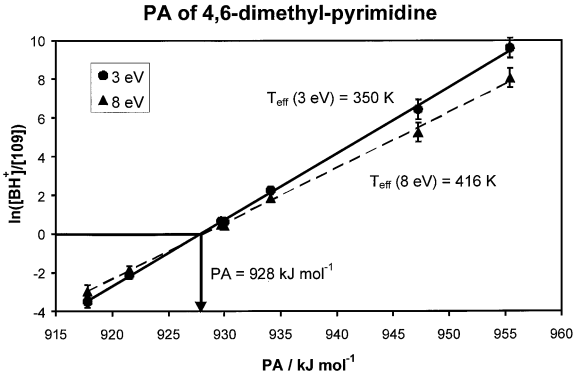

Fig. 5. Kinetic method plot for 4,6-dimethyl-pyrimidine. Reference molecules and proton affinities (in kJ mol^{-1}) are *n*-propylamine (917.8), *n*-butylamine (921.5), *sec*-butylamine (929.7), pyridine (930.0), *t*-butylamine (934.1), 4-methyl-pyridine (947.2), and 3,5-dimethyl-pyridine (955.4).

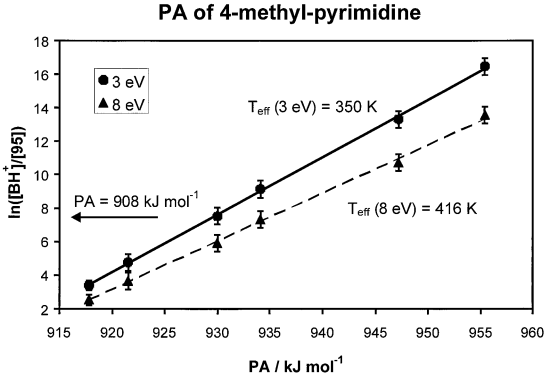

Fig. 6. Kinetic method plot for 4-methyl-pyrimidine.

4,6-dimethyl-pyrimidine

$$= 928 \pm 1 \text{ kJ mol}^{-1} (221.8 \pm 0.2 \text{ kcal mol}^{-1})$$

4-methyl-pyrimidine

$$= 908 \pm 2 \text{ kJ mol}^{-1} (217.0 \pm 0.5 \text{ kcal mol}^{-1})$$

The errors produced by the linear regression routine are ± 1 kJ mol^{-1} and ± 2 kJ mol^{-1} for 4,6-dimethyl-pyrimidine and 4-methyl-pyrimidine, respectively. The real uncertainties in the determinations are expected to be higher. The absolute proton affinities of the references are subject to uncertainties of approximately 4 kJ mol^{-1} (1 kcal mol^{-1}), although the *relative* affinities are frequently known to within 1 kJ mol^{-1} (0.2 kcal mol^{-1}). Cooks et al. generally quote uncertainties of ± 0.3 kcal mol^{-1} (1.25 kJ mol^{-1}) for data that vary by 5% in one point but show poorer correlation [16]. The uncertainty in the proton affinity of 4-methyl-pyrimidine is higher than that for 4,6-dimethyl-pyrimidine because it has been obtained from extrapolation rather than being bracketed by references. Attempts to remedy this deficiency using 3-chloropyridine (PA = 215.7 kcal mol^{-1}) as a reference failed. Fragmentation of pyridine/3-chloropyridine proton-bound dimers gave much smaller ratios than expected. In experiments on CN^+-bound dimers involving 3-chloropyridine, Yang et al. [17] reported similar anomalous results that were attributed to interfering ring addition reactions.

4.2. Calculations of proton affinities

Proton affinities for 4,6-dimethyl-pyrimidine and 4-methyl-pyrimidine were calculated via ab initio molecular orbital theory, to provide a point of comparison for the experiments. The proton affinities of several previously measured species, including some that are structurally similar to the unknowns, were also calculated to assess the reliability of the computational results.

The proton affinity is defined as the negative of the enthalpy of the reaction:

$$B + H^+ \rightarrow BH^+$$

This definition is expanded in Eq. (2):

$$PA = -\{H_f(BH^+) - H_f(B) - H_f(H^+)\} \quad (2)$$

$$= -\{E(BH^+) + E_T(BH^+) - E(B) - E_T(B)\} + \frac{5}{2}RT$$

where $E(BH^+)$, $E(B)$ are the electronic energies of the respective species, E_T is the correction to temperature T, and R is the gas constant.

E_T includes the zero-point vibrational energy (ZPVE) and the population of energy levels at temperature T. Because it is only the difference between these quantities for very similar molecules that is required, only the zero-point vibrations need be considered. Translational and rotational differences are very small and the vibrational difference generally falls below the accuracy of computation, and below the uncertainty of experiment. The $\frac{5}{2}RT$ term allows for the loss of the translational energy of H^+ ($\frac{3}{2}RT$) and the P-V work involved in changing from 2 particles to 1 for an ideal gas (RT).

Geometry optimizations were performed at the MP2/6-31G** level of theory. Analytical derivatives calculated at the optimized geometries, and with the same level of theory, were used to obtain the vibrational frequencies. These frequencies were scaled by a factor of 0.94 for calculating zero-point energies and thermal corrections [18]. Electronic energies were obtained from MP2/6-311+G(2df,2pd) single-point

Table 1
Calculated proton affinities for some molecules relevant to this study. Two values are shown for 4-methyl-pyrimidine. The numbers in parentheses indicate the site of *N*-protonation in each case

Molecule	MP2/6-31G**	MP2/6-311+G(2df,2pd)	Experimental
CH_4	540 (129.1)	542 (129.6)	544 (129.9)
NH_3	888 (212.3)	853 (204.0)	854 (204.0)
CH_3NH_2	930 (222.2)	900 (215.0)	899 (214.9)
tert-butylamine	961 (229.6)	932 (222.7)	934 (223.3)
pyridine	951 (227.4)	925 (221.1)	930 (222)
pyrimidine	902 (215.6)	879 (210.1)	886 (211.7)
4,6-dimethyl-pyrimidine	940 (224.7)	918 (219.3)	928 (221.8)
4-methyl-pyrimidine (1)	923 (220.5)	900 (215.1)	908 (217.0)
4-methyl-pyrimidine (3)	921 (220.1)	898 (214.7)	

Values reported as kJ mol^{-1}. Numbers in parentheses are in kcal mol^{-1}.

calculations at the MP2/6-31G** optimized geometries. This level of theoretical treatment (MP2/6-311+G(2df,2pd) // MP2/6-31G**) has been used in proton affinity calculations by Uggerud [18]. The calculated proton affinities (at 298 K) are shown in Table 1.

Calculated affinities match the database values for smaller molecules quite well. The values for pyridine and pyrimidine however are too low by approximately 5 kJ mol^{-1}. The values for 4,6-dimethyl-pyrimidine and 4-methyl-pyrimidine are also low in comparison to those obtained in the experiments described above. However if one compares the calculated and experimental affinities *relative* to pyrimidine, theory and experiment are in reasonable agreement.

4.3. The 6-methyl-pyrimidin-4-yl radical

Because the proton-bound dimers for the kinetic method experiments were created by ion/molecule reactions and not in a CI source it was possible to form them by two routes, depending on which species was used as the $[M + H]^+$ ion and which was used as the neutral reagent. When the dimer was formed by reacting neutral 4,6-dimethyl-pyrimidine with protonated pyridine, subsequent fragmentation produced the ratio used in the previous section for determining the proton affinity of 4,6-dimethyl-pyrimidine. However the reverse reaction, neutral pyridine with protonated 4,6-dimethyl-pyrimidine, produced three separate products in the region of the proton-bound dimer (*m/z* 188), at *m/z* 186, *m/z* 187, and *m/z* 188. Collisional activation of the *m/z* 188 ion produces *m/z* 109 and *m/z* 80 in the expected ratio for 4,6-dimethyl-pyrimidine and pyridine. Activation of the *m/z* 186 ion produces only *m/z* 107. The fragments of the *m/z* 187 ion are *m/z* 108 and *m/z* 80 as shown in Fig. 7.

A possible explanation of this result is the formation of alkyl pyridines and their inclusion in proton- or methyl cation-bound dimers, although this would require a rather convoluted and therefore unlikely mechanism. A proton-bound dimer of pyridine and a dimethyl-pyridine should fragment to give exclusively *m/z* 108 because the proton affinity difference

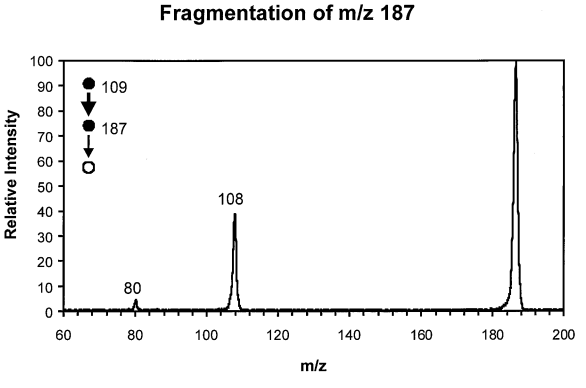

Fig. 7. Fragmentation spectrum of the *m/z* 187 ion produced by the reaction of 4,6-dimethyl-pyrimidine + H^+ and pyridine. In the upper left corner, filled circles represent a mass analyzer set to transmit a fixed mass (Q1 and Q3), whereas the open circle represents the final analyzer (Q5) that scans over the mass range of interest.

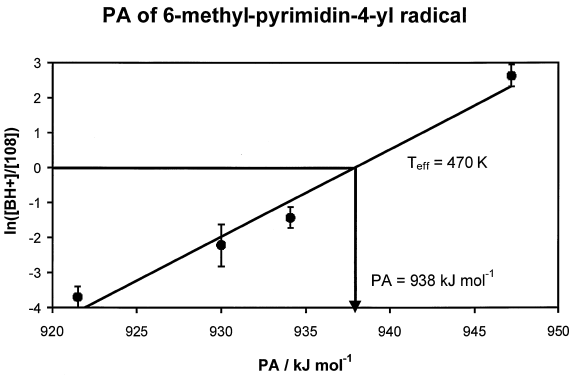

Fig. 8. Kinetic method plot for the 6-methyl-pyrimidin-4-yl radical.

is so large. McMahon et al. [19] have shown that relative methyl cation affinities for amines are approximately the same as proton affinities. Therefore a methyl cation-bound dimer of pyridine and a methylpyridine should fragment to *m/z* 108 and *m/z* 94 in a ratio similar to that observed for proton-bound dimers (approximately 200:1). This is clearly not the case.

Because alkylated pyridines have been discounted as candidates for the *m/z* 108 peak, it seems that it most likely results from protonated 4,6-dimethylpyrimidine via a hydrogen atom loss. The dimer is therefore either a ring-substituted $[M + H]^+$ ion or the proton-bound dimer of a radical species. A substitution reaction replacing hydrogen with pyridine on the pyrimidine ring could explain the formation of *m/z* 187, but it seems unlikely that such a structure should fragment to give *m/z* 80 under the relatively mild activation conditions employed. A more reasonable explanation is the formation of a radical, via a hydrogen atom loss, resulting in a proton-bound dimer of the radical and pyridine. Fragmentation of this dimer would produce protonated pyridine (*m/z* 80) and the *N*-protonated 6-methyl-pyrimidin-4-yl radical (*m/z* 108).

Similar results to those described above for experiments with pyridine were obtained with other reference compounds. Fig. 8 presents the data in the form of a kinetic method plot, with the results referring to direct pairings only. A large error bar is shown for the experiments involving pyridine as the reference base. The ratios obtained for this reference appeared to fall into two separate ranges. The correlation is not particularly good and the plot seems to have some curvature. The effective temperature parameter is also quite different from the previous results. This is not surprising because the value of this parameter does not depend on the activation conditions alone, but also on the stability of the dimer itself.

Overall, the data are less consistent than for the even-electron species but provide an estimate of 938 ± 4 kJ mol^{-1} (224 ± 1 kcal mol^{-1}) for the proton affinity of the radical. Several postulated structures for the *m/z* 108 radical ion (1–3) and the corresponding 107 Da neutral (4–6) are shown in Fig. 9.

Table 2 shows the calculated proton affinities for three sites (**1–3**) on the 6-methyl-pyrimidin-4-yl radical (**6**) and two alternative radicals (**4,5**). These values were calculated in a similar manner to those in the preceding section, except that the UMP2/6-311+G(2df,2pd) // UMP2/6-31G** level of theory was employed. The actual energies used were those obtained after projection of the first spin contaminant, i.e. PUMP2. Zero-point energies and thermal corrections were calculated from UHF/6-31G** frequencies, at the UHF/6-31G** optimized geometry, scaled by the usual factor of 1/1.12 (0.8929).

The mixing of different levels of theory in this manner is undesirable, but the available computational resources prohibited the calculation of UMP2/6-31G** frequencies. In any case, as the widespread use of scaling factors indicates, the calculated zero-point energies are only estimates and, as such, it seems reasonable to use the UHF/6-31G** frequencies in this case.

N-Protonation of the radical (**6/2** and **6/3** in Table 2) is the only structure that gives a proton affinity consistent with the experimental observations.

The energies of the relevant structures are shown in Table 3. These results predict the protonated radicals, **2** and **3**, to be more stable than the formal structure of the molecular ion, **1**. This can be rationalized as being due to resonance stabilization of the $CH_2^{\cdot}$ group, as in the case of the benzyl radical. The optimized structures of both the neutral and the molecular ion have a single proton in each methyl

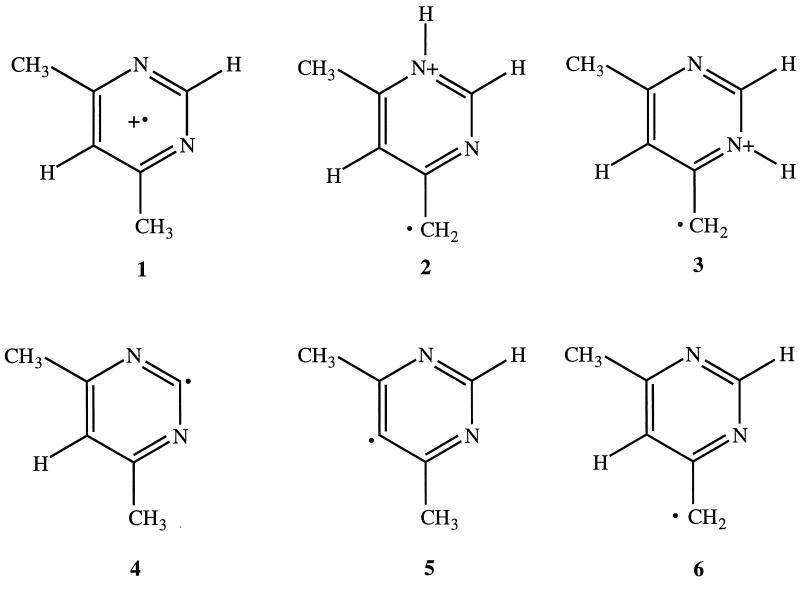

Fig. 9. Possible structures for the *m/z* 108 ion and 107 Da neutral.

group lying in the plane of the ring and directed towards the relevant nitrogen atom. Rearrangement of the molecular ion to the protonated radical form should thus be facile and could occur after ionization in the source or upon collisional activation with the neutral reagent gas.

The proton affinities of other radical species have previously been determined by Cooks et al. using the kinetic method [16,20]. Among the species studied were a number of cresol isomers that produced evidence for the formation of benzylic radicals similar to those proposed in this study.

All these lines of evidence point to the conclusion that the *N*-protonated 6-methyl-pyrimidin-4-yl radical is produced in the first reaction region, and undergoes further reactions to produce proton-bound dimers. Using the kinetic method the proton affinity of the radical is estimated as 938 ± 4 kJ mol^{-1} (224 ± 1 kcal mol^{-1}). This is in good agreement with the calculated values: 928 kJ mol^{-1} (221.8 kcal mol^{-1}), for **6/3**, and 933 kJ mol^{-1} (223.1 kcal mol^{-1}), for **6/2**.

5. Conclusions

Proton affinities have been determined for 4,6-dimethyl-pyrimidine (928 ± 1 kJ mol^{-1}) and 4-methyl-pyrimidine (908 ± 2 kJ mol^{-1}) via the kinetic

Table 2
Calculated proton affinities for 4,6-dimethyl-pyrimidine−H radicals

B/BH^+	PUMP2/6-31G**// UHF/6-31G**	PUMP2/6-31G**// UMP2/6-31G**	PUMP2/6-311+G(2df,2pd)// UMP2/6-31G**
6/1	812 (194.1)	821 (196.2)	791 (189.0)
6/2	946 (226.2)	957 (228.7)	933 (223.1)
6/3	939 (224.4)	951 (227.3)	928 (221.8)
4/1	889 (212.5)	893 (213.4)	863 (206.3)
5/1	913 (218.1)	923 (220.5)	895 (213.9)

Values in kJ mol^{-1} (values in parentheses in kcal mol^{-1}).

Table 3
Calculated energies for structures **1–6**. In the final column, ZPVE represents the vibrational energy at 300 K, including zero-point vibrational energy

Species	PUMP2/6-31G**// UHF/6-31G**	PUMP2/6-31G**// UMP2/6-31G**	PUMP2/ 6-311+G(2df,2pd) //UMP2/6-31G**	ZPVE// UHF/6-31G**
1	−341.58887	−341.58731	−341.89660	0.13316
2	−341.64083	−341.64002	−341.95188	0.13410
3	−341.63790	−341.63770	−341.94956	0.13398
4	−341.24085	−341.23774	−341.55833	0.12134
5	−341.23190	−341.22651	−341.54623	0.12137
6	−341.26874	−341.26389	−341.58461	0.12006

method. The versatility of the pentaquadrupole instrument was demonstrated through the discovery of alternative reaction products in a reversed ion/molecule reaction that lead to an estimate for the proton affinity of the 6-methyl-pyrimidin-4-yl radical of 938 ± 4 kJ mol^{-1}.

Acknowledgements

P.D.T. acknowledges the assistance of the Australian Government through an APRA (APA) Scholarship during his graduate studies and the advice of Professor Jim Morrison, particularly as a temporary research supervisor. R.J.S.M. thanks the Australian Research Council (ARC) for a small ARC grant that was of great help in the early days of constructing the pentaquadrupole mass spectrometer and more recently for ongoing large ARC support.

References

[1] K.L. Busch, G.L. Glish, S.A. McLuckey, Mass Spectrometry/ Mass Spectrometry: Techniques and Applications of Tandem Mass Spectrometry, VCH, New York, 1988.
[2] A.G. Marshall, C.L. Hendrickson, G.S. Jackson, Mass Spectrom. Rev. 17 (1998) 1.
[3] R.E. March, J. Mass Spectrom. 32 (1997) 351.
[4] K.P. Bateman, S.J. Locke, D.A. Volmer, J. Mass Spectrom. 32 (1997) 297.
[5] J.A. Loo, C.G. Edmonds, R.D. Smith, Anal. Chem. 63 (1991) 2488.
[6] D.J. Burinsky, R.G. Cooks, E.K. Chess, M.L. Gross, Anal. Chem. 54 (1982) 295.
[7] J.C. Schwartz, A.P. Wade, C.G. Enke, R.G. Cooks, Anal. Chem. 62 (1990) 1809.
[8] M.N. Eberlin, Mass Spectrom. Rev. 16 (1997) 113.
[9] R.G. Cooks, T.L. Kruger, J. Am. Chem. Soc. 99 (1977) 1279.
[10] R.G. Cooks, J.S. Patrick, T. Kotiaho, S.A. McLuckey, Mass Spectrom. Rev. 13 (1994) 287.
[11] R.G. Cooks, P.S.H. Wong, Acc. Chem. Res. 31 (1998) 379.
[12] P.D. Thomas, A Pentaquadrupole Mass Spectrometer for MS^3 and Ion/Molecule Reaction Studies, Ph.D. Thesis, Monash University, 1998.
[13] D.A. Dahl, SIMION 3D, Lockheed Idaho Engineering Technologies, 1996.
[14] M.J. Frisch, G.W. Trucks, H.B. Schlegel, P.M.W. Gill, B.G. Johnson, M.A. Robb, J.R. Cheeseman, T. Keith, G.A. Petersson, J.A. Montgomery, K. Raghavachari, M.A. Al-Laham, V.G. Zakrzewski, J.V. Ortiz, J.B. Foresman, J. Cioslowski, B.B.B. Stefanov, A. Nanayakkara, M. Challacombe, C.Y. Peng, P.Y. Ayala, W. Chen, M.W. Wong, J.L. Andres, E.S. Replogle, R. Gomperts, R.L. Martin, D.J. Fox, J.S. Binkley, D.J. Defrees, J. Baker, J.P. Stewart, M. Head-Gordon, C. Gonzalez, J.A. Pople, GAUSSIAN 94, Revision D.3, Gaussian, Inc., Pittsburgh, PA, 1995.
[15] E.P.L. Hunter, S.G. Lias, J. Phys. Chem. Ref. Data 27 (1998) 413.
[16] S.H. Hoke II, S.S. Yang, R.G. Cooks, D.A. Hrovat, W.T. Borden, J. Am. Chem. Soc. 116 (1994) 4888.
[17] S.S. Yang, O. Bortolini, A. Steinmetz, R.G. Cooks, J. Mass Spectrom. 30 (1994) 184.
[18] E. Uggerud, J. Am. Chem. Soc. 116 (1994) 6873.
[19] T.B. McMahon, T. Heinis, G. Nicol, J.K. Hovey, P. Kebarle, J. Am. Chem. Soc. 110 (1988) 7591.
[20] G. Chen, N. Kasthurikrishnan, R.G. Cooks, Int. J. Mass Spectrom. Ion Processes 151 (1995) 69.